

Article

# EMG and IMU Data Fusion for Locomotion Mode Classification in Transtibial Amputees

Omar A. Gonzales-Huisa <sup>1</sup>, Gonzalo Oshiro <sup>2</sup>, Victoria E. Abarca <sup>3</sup>, Jorge G. Chavez-Echajaya <sup>4</sup>  
and Dante A. Elias <sup>3,\*</sup>

<sup>1</sup> Faculty of Science and Engineering, Electronic Engineering, Pontificia Universidad Católica del Perú, Lima 15088, Peru; gonzales.omar@pucp.edu.pe

<sup>2</sup> Faculty of Science and Engineering, Mechatronics Engineering, Pontificia Universidad Católica del Perú, Lima 15088, Peru; gonzalo.oshiro@pucp.edu.pe

<sup>3</sup> Biomechanics and Applied Robotics Research Laboratory, Pontificia Universidad Católica del Perú, Lima 15088, Peru; victoria.abarca@pucp.edu.pe

<sup>4</sup> Faculty of Science and Engineering, Biomedical Engineering, Pontificia Universidad Católica del Perú, Lima 15088, Peru; jorge.chaveze@pucp.edu.pe

\* Correspondence: delias@pucp.pe

**Abstract:** Despite recent advancements in prosthetic technology, lower-limb amputees often remain limited to passive prostheses, which leads to an asymmetric gait and increased energy expenditure. Developing active prostheses with effective control systems is important to improve mobility for these individuals. This study presents a machine-learning-based approach to classify five distinct locomotion tasks: ground-level walking (GWL), ramp ascent (RPA), ramp descent (RPD), stairs ascent (SSA), and stairs descent (SSD). The dataset comprises fused electromyographic (EMG) and inertial measurement unit (IMU) signals from twenty non-amputated and five transtibial amputated participants. EMG sensors were strategically positioned on the thigh muscles, while IMU sensors were placed on various leg segments. The performance of two classification algorithms, support vector machine (SVM) and long short-term memory (LSTM), were evaluated on segmented data. The results indicate that SVM models outperform LSTM models in accuracy, precision, and F1 score in the individual evaluation of amputee and non-amputee datasets for 80–20 and 50–50 data distributions. In the 80–20 distribution, an accuracy of 95.46% and 95.35% was obtained with SVM for non-amputees and amputees, respectively. An accuracy of 93.33% and 93.30% was obtained for non-amputees and amputees by using LSTM, respectively. LSTM models show more robustness and inter-population generalizability than SVM models when applying domain-adaptation techniques. Furthermore, the average classification latency for SVM and LSTM models was 19.84 ms and 37.07 ms, respectively, within acceptable limits for real-time applications. This study contributes to the field by comprehensively comparing SVM and LSTM classifiers for locomotion tasks, laying the foundation for the future development of real-time control systems for active transtibial prostheses.



**Citation:** Gonzales-Huisa, O.A.; Oshiro, G.; Abarca, V.E.; Chavez-Echajaya, J.G.; Elias, D.A. EMG and IMU Data Fusion for Locomotion Mode Classification in Transtibial Amputees. *Prosthesis* **2023**, *5*, 1232–1256. <https://doi.org/10.3390/prosthesis5040085>

Academic Editor: Arnab Chanda

Received: 20 October 2023

Revised: 15 November 2023

Accepted: 16 November 2023

Published: 21 November 2023

**Keywords:** electromyography; inertial sensor; long short-term memory; support vector machine; transtibial prosthesis



**Copyright:** © 2023 by the authors. Licensee MDPI, Basel, Switzerland. This article is an open access article distributed under the terms and conditions of the Creative Commons Attribution (CC BY) license (<https://creativecommons.org/licenses/by/4.0/>).

## 1. Introduction

The number of patients undergoing amputations is increasing annually in the Western world, with 90% of these cases related to lower-limb amputations [1] (p. 5). In the United States, it is estimated that over 185,000 individuals experience some form of amputation each year [2], with more than 150,000 of these cases involving lower-limb amputations [3]. Lower-limb amputations are a significant cause of locomotor [4] and functional difficulty for the individual, leading to physical, psychological, family, and personal impacts [5]. Additionally, it has been observed that in transtibial amputees, the loss of ankle power

generation increases metabolic energy costs by 20–30% [6]. This situation raises the risk of musculoskeletal problems and falls [7].

Despite advances in prosthetic technology in recent years, many people with lower-limb amputations are limited to passive prostheses that result in asymmetric gait and require more significant energy expenditure from the user [6,8]. The incapacity of passive prostheses to generate energy limits the abilities of both transfemoral and transtibial amputees to move appropriately during daily activities [9]. Tasks such as ascending ramps or climbing stairs require net-positive power outputs that are not entirely achievable with passive prostheses [10].

In order to address these challenges, the development of active prosthetics has become one of the primary objectives [8,10]. These prosthetics must be able to deliver the appropriate power and mechanical torque, potentially assisting amputees in various locomotion activities, not limited exclusively to level walking [9]. Developing a control system that allows a transtibial prosthesis to replicate the walking abilities of a healthy individual and adapt naturally to different terrains remains a significant challenge [11]. For some commercially available active lower-limb prostheses, amputees need to instruct their motion intention to the prosthesis through buttons or by executing a non-natural movement [12]. Therefore, it is necessary to develop control systems containing algorithms that can automatically detect a user's movement intention during various locomotion activities to manage an active transtibial prosthesis [13,14].

The commonly used sensors for movement intention recognition are electromyography (EMG) sensors or inertial measurement units (IMU) [4]. EMG sensors have the potential to achieve a high range of voluntary control over the prosthesis and represent the earliest signal that can be extracted during motor activities [15]. On the other hand, using IMU sensors allows for identifying the gait cycle phase in conjunction with other mechanical sensors like contact switches or load cells [11,12,15]. Some studies have fused the data provided by both types of sensors, as seen in the case of Barberi et al. [15], who developed a locomotion task classification algorithm for transfemoral prosthesis comparing support vector machine (SVM) algorithms with a linear or second-order polynomial kernel. Four EMG sensors located in the muscles of the amputated leg, three IMU sensors, and contact switches for data collection were used to achieve an accuracy greater than 94%. Zhou et al. [16] fused data from three EMG signals and one IMU inertial signal to develop an ankle-movement-recognition system on non-amputees. Different algorithms were compared in this study, with SVM being the traditional algorithm with the best performance and bi-directional long short-term memory (BiLSTM) being the algorithm with the overall best performance at 99.8%. Meng et al. [17] collected EMG and inertial signals from ten non-amputee subjects to train classification algorithms for seven locomotion activities. They performed a fusion of EMG and IMU data and tested it on four classification algorithms: support vector machine (SVM), K-nearest neighbor (KNN), artificial neural network (ANN), and linear discriminant analysis (LDA). The fusion of the EMG signals improved the accuracy of steady-state locomotion-activity recognition by using SVM from 90% (using only acceleration data) to 98% (using the data fusion of EMG + IMU). Hu et al. [18] propose using their dataset to develop control strategies for motion-intention recognition by using EMG and IMU data-fusion techniques focused on machine learning classification. Given the ongoing introduction of new sensors, the fusion of technologies for motion recognition is a hotspot in the field of prosthetic-control research [16].

The existing literature includes studies that evaluate ankle movements in transtibial amputees by using EMG sensors placed on muscles of the leg segment (such as the tibialis anterior and gastrocnemius) [19,20]. However, the majority of transtibial amputees, especially in developing countries, use a socket-suspended prosthesis [21,22]. This socket type makes it challenging to position EMG sensors and increases the risk of displacement by constant friction [6]. Additionally, comparative studies involving SVM and LSTM have been found, but the participants evaluated are people without any mobility impairment or locomotion disorder [7,16,17].

This study illustrates the influence of integrating EMG and IMU signal data on classifying five locomotion tasks among individuals with and without transtibial amputations. The evaluated locomotion activities include walking on a flat surface, an incline/decline ramp, and ascending/descending stairs. A comparison between two classification models, support vector machine (SVM) and long short-term memory (LSTM), both of which have shown optimal results in previous research, is presented [6,7,14–17]. The significant contributions of this work are as follows:

- The fusion of two critical signals, EMG and IMU, significantly enhanced locomotion task classification.
- A comprehensive comparison between two powerful classification models, SVM and LSTM, tailored explicitly for transtibial amputees across a spectrum of locomotion activities.
- A methodology to identify the most representative muscles on the thigh in the gait cycle of individuals with transtibial amputations who use prosthetic sockets on the residual limb was elaborated.
- The use of domain-adaptation techniques to enhance the developed models' adaptability and robustness, ensuring the models' reliability and effectiveness across diverse locomotion patterns.

## 2. Materials and Methods

### 2.1. Experiment Setup

This study was conducted at the Biomechanics and Applied Robotics Laboratory at the Pontificia Universidad Católica del Perú. It was approved by the Ethics Committee for Research in Life Sciences and Technologies of the same institution (approval number 073-2023-CEICVyT/PUCP). A total of 5 male participants with transtibial amputations (Group A) and 24 participants without amputations (12 males and 12 females, Group B) were recruited for this study. Group A had an average age of  $38.6 \pm 16.36$  years, weight of  $76.00 \pm 11.64$  kg, and height of  $172.04 \pm 6.24$  cm. Table 1 shows more detailed background information for this group. Group B had an average age of  $22.125 \pm 2.51$  years, weight of  $62.56 \pm 11.39$  kg, and height of  $164.92 \pm 9.34$  cm. All the participants provided written informed consent before the experiment.

**Table 1.** Transtibial amputee subjects' characteristics (age, height, weight, amputated side, years since amputation, and current prosthesis).

Participant	Age (Years)	Height (cm)	Weight (kg)	Amputated Side	Year since Amputation	Current Prosthesis
Amputee 01	58	167	66	Right	17 years/2006	Transtibial prosthesis with acrylic sock-type socket with liner and rigid foot
Amputee 02	50	167	79	Left	5 years/2018	Transtibial plastic socket type prosthesis without liner and articulated foot
Amputee 03	24	170	70	Right	1.5 years/2022	Transtibial fiberglass prosthesis with resin, socket type with liner and articulated foot
Amputee 04	20	174	70	Right	2 years/2021	Transtibial carbon fiber socket-type prosthesis with liner and rigid foot
Amputee 05	41	182	95	Right	12 years/2011	Transtibial carbon fiber socket-type prosthesis with liner and rigid foot

Selection criteria were established to ensure that participants in both groups met the requirements for this study. For Group A, the inclusion criteria included a minimum stump length of 12.7 cm, possession of a well-maintained transtibial prosthesis, the ability to walk independently, and a non-congenital amputation. For Group B, the inclusion criteria included regular physical activity to facilitate the identification of evaluated muscles and the absence of any motor or pathological limitation significantly affecting their gait. A licensed occupational therapist provided support in validating the selection criteria. All participants underwent an evaluation to confirm that they met the selection criteria. These criteria were established to ensure that the study results were valid and reliable and that the participants represented the target population.

EMG signals were captured from four muscles in the right thigh, as shown in Table 2 and Figure 1: rectus femoris (RF), biceps femoris (BF), tensor fascia latae (TF), and adductor longus (AL). In addition, IMU signals were captured from the sensor placed on the rectus femoris (RF), the tibia (TB), and the instep on the foot (FT) [15]. The sensors were placed on the muscles through palpation while participants performed specific muscle activation movements, as detailed in Table 2. A set of six Trigno Avanti wireless non-invasive surface sensors from DELSYS was used for this purpose [23].

**Table 2.** Movements for muscle detection during EMG sensor positioning.

Muscle	Movement
Rectus femoris (RF)	With the hip slightly flexed, perform knee extension movements.
Biceps femoris (BF)	With the hip slightly extended, perform knee flexion movements, bringing the heel towards the gluteus.
Tensor fasciae latae (TF)	Perform hip abduction movements from a natural position.
Adductor Longus (AL)	With the feet at hip level, rest the inside edge of the foot against the floor.

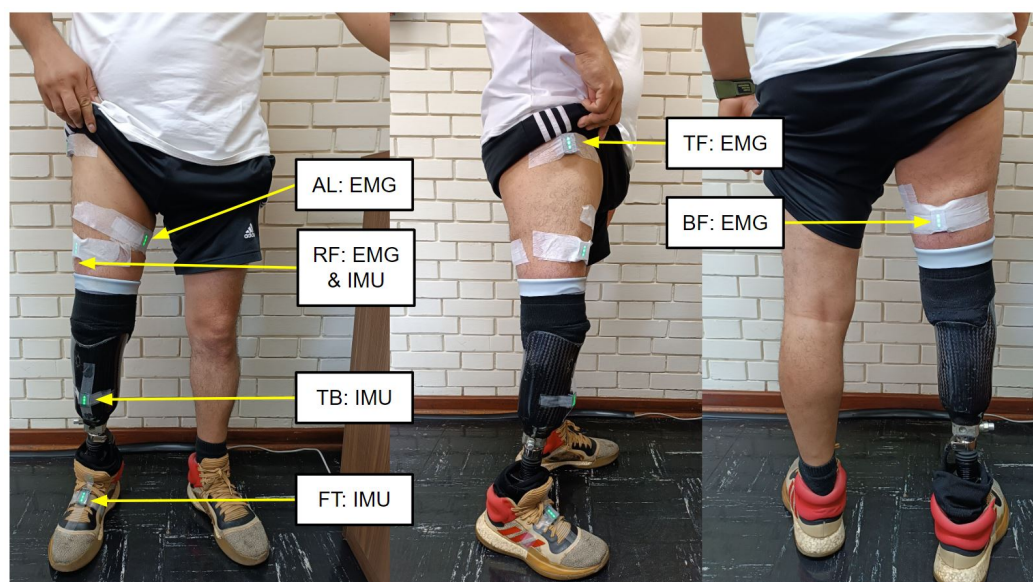


**Figure 1.** Experiment setup for data collection. The participant wore a set of sensors. EMG electrodes were placed on four muscles—rectus femoris (RF), biceps femoris (BF), tensor fascia latae (TF), and adductor longus (AL). Inertial sensors were placed on the rectus femoris (RF), tibia (TB), and the foot (FT).

## 2.2. Experimental Protocol and Tests

Before starting data collection, the sensors were positioned and the participants were instructed to perform short walks to verify the correct capture of the signals by the sensors. Once the proper functioning of the sensors was confirmed, data collection proceeded. Five

locomotion activities were addressed in this study, namely ground-level walking (GLW), ramp ascent (RPA), ramp descent (RPD), stairs ascent (SSA), and stairs descent (SSD). Activities were performed in three different common-use environments. A six-meter ramp with a 7° slope was designated as the first environment for up/down walking activities. A 10 m flat surface was selected as the second environment for ground-level walking. Finally, 11 steps, each 16 cm high, were designated as the third environment for the stair ascent and descent trials. It should be noted that the environments comply with the A.120 standard of the Ministry of Housing, Construction and Sanitation of the Peruvian government [24]. Each activity was repeated ten times, totaling 50 tests per participant. The participants completed each test at a walking speed that was comfortable for them. A participant undergoing data-collection trials is shown in Figure 2.

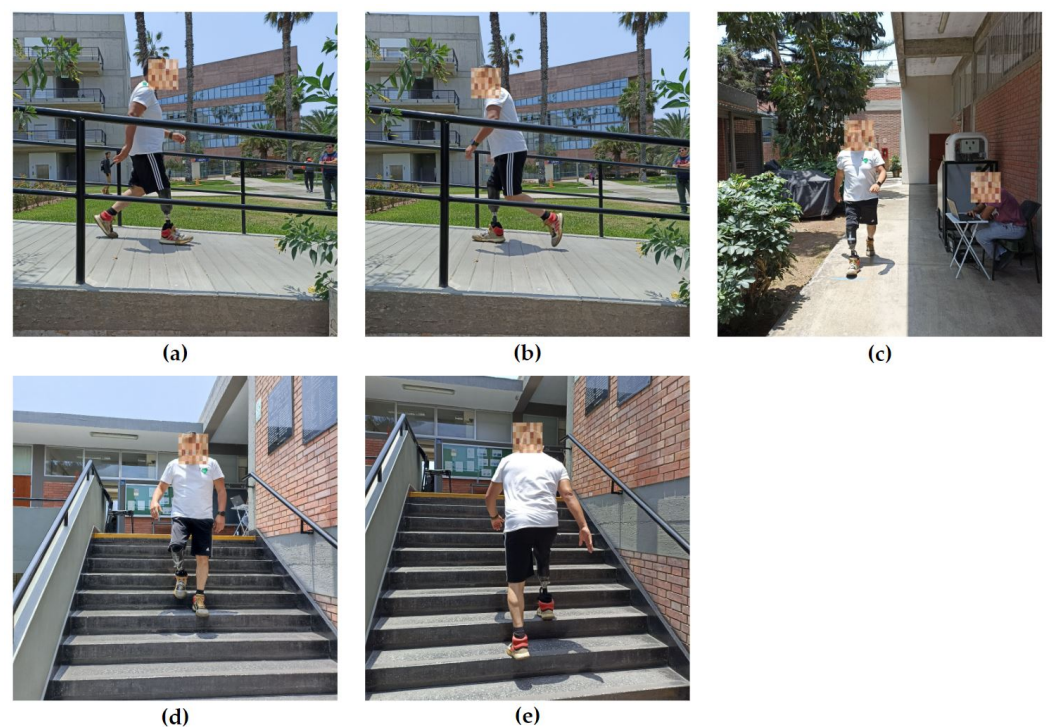


**Figure 2.** Participant undergoing data-collection trials. (a) Ramp ascent; (b) ramp descent; (c) ground-level walking; (d) stair ascent; (e) stair descent.

### 2.3. Data Processing

The raw EMG signals were collected at a sampling frequency of 1259 Hz, capturing a range of  $\pm 5.5$  mV and using a band-pass filter of 20–450 Hz. The inertial signals were collected at a sampling rate of 148 Hz, with an accelerometer range of  $\pm 16$  g and a gyroscope range of  $\pm 2000$  dps. All the sensors were configured as EMG+IMU in the data-acquisition EMGWorks Acquisition software version 4.8.0, developed by Delsys, to capture both electromyographic and inertial signals. Figure 3 shows an example of the EMG signals captured during the stair descent of a participant with a transtibial amputation, and Figure 4 shows an example of the EMG signals captured from the same participant during ramp descent.

The Delsys File Utility tool converts the acquired signals from .hpf to .mat format. A MATLAB-R2021a code was developed on a 2x Nvidia GeForce RTX 2080, Intel(R) Core(TM) i7-9700K Processor, and a 64.0 GB RAM computer to organize the raw data from each trial per participant in a way that allows the EMG and IMU information to be visualized by the sensor. Also, the columns not used in the algorithm's training were removed. Each trial per participant contains 16 features, including the EMG signals from the sensors located in the BF, TF, RF, and AL and the inertial signals from the sensors located in the RF, tibia, and foot.

The features from each trial per participant were converted to .csv format for further use in algorithm training. Simultaneously, the EMGWorks Analysis software version 4, developed by Delsys, manually sets each trial's start and end times, ensuring the participant performs the evaluated activity during the segmented time interval.

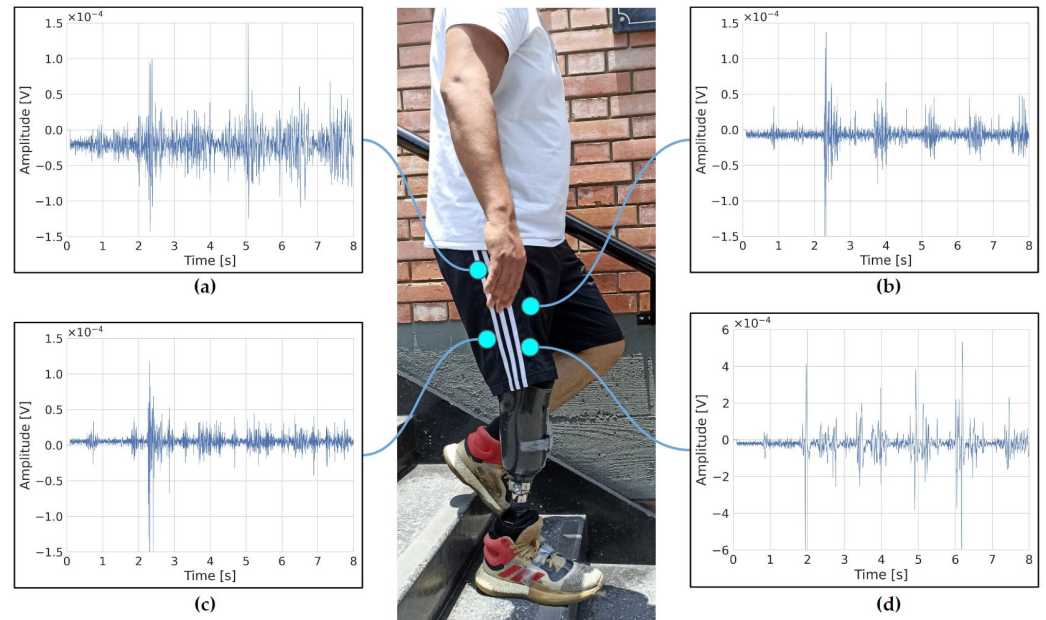


**Figure 3.** EMG signals of the four muscles evaluated from a transtibial amputation participant while performing the stairs descent task (SSD). (a) Raw EMG signal corresponding to the tensor fasciae latae (TF) muscle. (b) Raw EMG signal corresponding to the adductor longus (AL) muscle. (c) Raw EMG signal corresponding to the biceps femoris (BF) muscle. (d) Raw EMG signal corresponding to the rectus femoris muscle (RF).

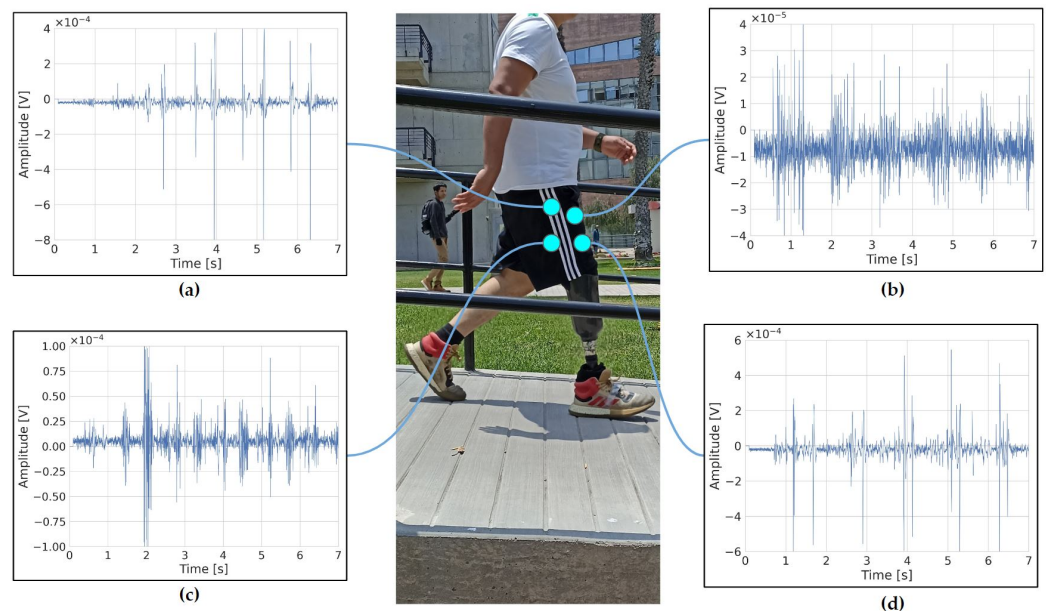


**Figure 4.** EMG signals of the four muscles evaluated from a participant with a transtibial amputation while performing the task of ramp descending (RPD). (a) Raw EMG signal corresponding to the tensor fasciae latae (TF) muscle. (b) Raw EMG signal corresponding to the adductor longus (AL) muscle. (c) Raw EMG signal corresponding to the biceps femoris (BF) muscle. (d) Raw EMG signal corresponding to the rectus femoris muscle (RF).

A peak-detection algorithm in Python processes the Z-axis acceleration data from the sensor located on the tibia to identify walking cycles within the segmented time interval. Literature-provided data show that the average duration between gait cycles varies between 0.8 and 1.6 s [14], a time-frame set as a constraint for peak detection as shown in Figure 5.

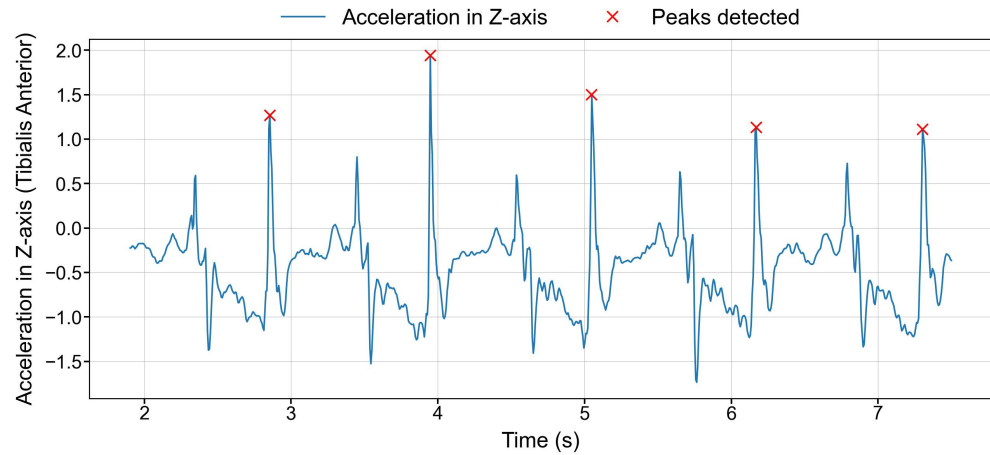


**Figure 5.** Graph of the Z-axis acceleration from the sensor corresponding to the tibia after being processed by the peak-detection algorithm. The interval between two consecutive ‘x’ marks corresponds to one gait cycle.

Identifying the gait cycles in each trial allows for segmenting the EMG and IMU data. The EMG and IMU datasets are segmented separately due to their different sampling frequencies. Four features are extracted from the EMG signals, including the mean absolute value (MAV), root mean square (RMS), standard deviation (SD), and waveform length (WL) [25]. The literature review demonstrates the importance of these features in a time-domain analysis [6,15–17,25,26]. In the case of inertial signals, only the MAV is extracted [4,15]. The feature-extracted EMG and IMU description was quantified by Equations (1)–(4):

$$\text{Mean Absolute Value (MAV)} = \frac{1}{N} \sum_{i=1}^N x(t_i) \tag{1}$$

$$\text{Root Mean Square (RMS)} = \sqrt{\frac{1}{N} \sum_{i=1}^N x(t_i)^2} \tag{2}$$

$$\text{Standard Deviation (SD)} = \sqrt{\frac{\sum_{i=1}^N (x_i - \bar{x})^2}{N}} \tag{3}$$

$$\text{Waveform Length (WL)} = \sum_{i=2}^N |x(t_i) - x(t_{i-1})| \tag{4}$$

A shorter EMG window length becomes fundamental for reducing the computational burden overall in tasks where the interaction between the human and the machine requires a real-time actuation [27]. Even though the EMG and IMU signals were sampled with different frequencies, by using a fixed window length of 80 ms [17,27,28] and overlapping of 40 ms for feature extraction, the same amount of data is finally obtained for both signals. These new signals are a low-frequency representation of the original signals. For example, for the RMS calculation, since a data point is obtained every 80 ms, after evaluating the entire trial timeline, the same amount of RMS data will be accepted for both EMG and IMU signals. Figure 6 depicts an example of sequence extractions.

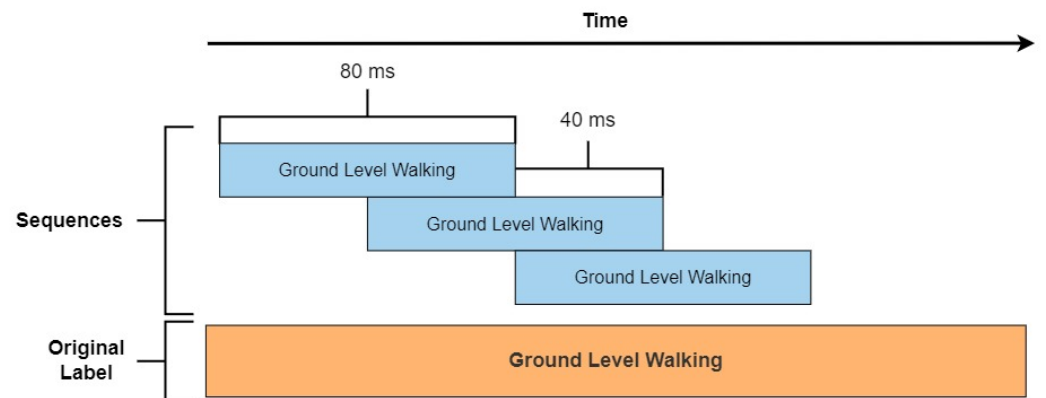


**Figure 6.** Example of sequence extraction. The gait cycle is represented in orange, and the blue sequences represent data segments of ground-level walking.

**2.4. System Architecture**

Two algorithms were employed: support vector machine (SVM) and long short-term memory (LSTM). SVM is a classical machine learning algorithm based on hyperplane separation in a higher-dimensional space, which renders it effective for non-linear classification problems. This algorithm has been employed in various studies for its low computational cost and high efficiency [6,14–17]. In this study, an SVM with an RBF kernel is employed. On the other hand, LSTM is a recurrent neural network algorithm whose primary concept involves regulating cell states by using input, forget, and output gates [16]. The architecture for LSTM in this study comprises an input layer followed by a bi-directional LSTM layer with 144 units, succeeded by a Dropout layer with a rate of 0.4. Subsequently, a second bi-directional LSTM layer with 72 units is implemented, followed by a Dropout layer with a rate of 0.4. Next, a dense layer with a ReLU activation function and 16 units is included, followed by a Softmax layer with five outputs for classification. The process followed by the LSTM algorithm is detailed in Figure 7.

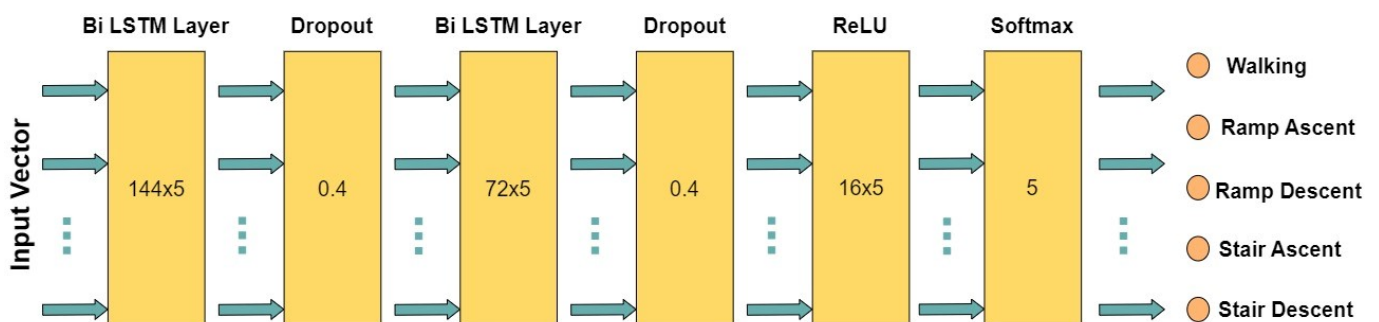


**Figure 7.** Architecture of the process performed by the LSTM algorithm, separated into layers.

**2.5. Data Analysis: Performance Metrics**

The proposed classifier model was evaluated by using accuracy, precision (P), recall (R), and the F1 score. *Accuracy* represents the proportion of accurate predictions out of the total predictions made. *Precision (P)* quantifies the proportion of true positives (Tp) that were indeed correct about the total positive predictions, minimizing false positives (Fp). *Recall* quantifies the proportion of true-positive (Tp) cases that the model accurately identified. This metric ensures that any true-positive case is inadvertently overlooked. The *F1 score* represents the proportion between precision (P) and recall (R). It is used for evaluating the algorithm’s performance, and its application helps mitigate substantial

imbalances between false positives ( $Fp$ ) and false negatives ( $Fn$ ). The performance metrics were quantified by Equations (5)–(8):

$$Accuracy = \frac{Tp + Tn}{Tp + Tn + Fp + Fn} \quad (5)$$

$$Precision = \frac{Tp}{Tp + Fp} \quad (6)$$

$$Recall = \frac{Tp}{Tp + Fn} \quad (7)$$

$$F1 \text{ score} = \frac{2PR}{P + R} \quad (8)$$

## 2.6. Hyperparameters

The primary hyperparameters used during the training of the SVM and LSTM models are described in this subsection. The computer setup is a 2x Nvidia GeForce RTX 2080, Intel(R) Core(TM) i7-9700K Processor, and 64.0 GB RAM.

### 2.6.1. Selection Methodology

The RandomizedSearchCV and GridSearchCV methodologies were used to acquire the optimal values for the hyperparameters. RandomizedSearchCV randomly groups hyperparameters from a large set and iterates them ten times for training and performance evaluations. The optimal combination of hyperparameters is selected by using five-fold cross-validation. A more specific range of values for the hyperparameters can be chosen due to the outputs of this methodology.

The GridSearchCV methodology exhaustively explores all possible combinations of the reduced set of hyperparameters. Three-fold cross-validation systematically examines each combination for training and validation, ultimately identifying the combination with the best performance.

### 2.6.2. Hyperparameters Selected for SVM

The kernel in SVM is a mathematical function that transforms data from their original domain to a higher-dimensional feature space. Three prominent kernel types were evaluated: linear, polynomial, and RBF. Among them, the radial basis function (RBF) kernel demonstrated superior performance within the algorithm. Another critical component of the SVM model is the C-SVM, a regularization parameter that dictates the permissible extent of training errors. In this implementation, the C-SVM was set to a value of 10.

### 2.6.3. Hyperparameters Selected for LSTM

For the LSTM model, several hyperparameters were meticulously selected to optimize its performance. The learning rate was set at 0.001 to ensure efficient convergence towards the global minimum and to prevent the model from getting stuck in local minima. The Adaptive Moment Estimation (Adam) optimizer was employed to adapt the model's weights during training. The loss function used was categorical cross-entropy, which quantifies the difference between the model's predictions and the actual training values, thereby serving as a performance metric during training. Regarding training epochs, the data were presented 200 times to the model. Early stopping criteria were also implemented; training would cease if the loss function in the validation data did not improve by a margin of 0.001 over ten consecutive epochs. The ModelCheckpoint feature was also used to preserve the model states that demonstrated superior performance throughout the training process.

### 2.7. Domain-Adaptation Techniques

In locomotion classification tasks, domain adaptation is vital to ensure robust models for cross-subject generalization. The core objective is to minimize performance gaps when applying a model to new subjects not encountered during training. This necessity arises from the inherent variability in human biomechanics, where individuals exhibit unique movement patterns and characteristics. Consequently, the challenge lies in ensuring that the trained model, which has learned from a specific dataset, can seamlessly extend its predictive capabilities to individuals not encountered during the training phase. Therefore, domain adaptation enhances the model's adaptability and minimizes performance disparities when confronted with diverse subjects. This is essential for the practical deployment of locomotion classification systems in real-world scenarios where encountering new subjects is inevitable.

Several domain-adaptation techniques are employed to address the challenges of cross-subject variability in locomotion classification. One prominent approach is transfer learning, where models are initially pre-trained on data from multiple subjects and subsequently fine tuned on a smaller dataset from a subject not included in the initial training set. This enables the model to leverage knowledge from diverse subjects while refining its predictive capabilities for the target subject. Another effective strategy involves feature-alignment techniques like correlation alignment (CORAL). This method aligns feature distributions across subjects, ensuring a harmonized representation of locomotion characteristics and minimizing discrepancies in the model's performance when applied to new individuals.

### 2.8. Statistical Analysis

Statistical analysis was performed by using an analysis of variance (ANOVA) to contrast the metrics obtained, such as the accuracy, precision, and F1 score, on the results. Performing this analysis is crucial to determine whether there is a significant difference when comparing the performance of the classification models used (SVM and LSTM) and the different groups of participants (amputees and non-amputees). However, the drawback lies in the fact that an ANOVA only indicates the presence of at least one distinct group when it detects a significant difference without specifying which one. Tukey's honest significant difference (HSD) post hoc methodology was applied after the ANOVA to identify the most significant mean differences between the groups to obtain a more detailed comparison.

The statistical analysis was carried out in several steps. In the data-preparation phase, separate groups were created for the SVM and LSTM models according to their performance metrics. Before the ANOVA application, assumption checks, including normality and the homogeneity of variances, were performed by using the Shapiro–Wilk test for normality and Levene's test for the homogeneity of variances in the assumption-verification stage. The ANOVA test was implemented for each performance metric (accuracy, precision, and F1 score) to identify the possible statistically significant differences between the two models. If the ANOVA detected significant differences, Tukey's honest significant difference (Tukey's HSD) post hoc test for paired comparisons was performed to determine which specific pairs of models showed significant differences.

### 2.9. Experimental Steps

An exhaustive set of experiments tailored to each dataset was conducted to evaluate the efficacy of the proposed classification models. The experiments were designed to address various aspects of model generalization and performance. Below are the specific experimental configurations:

1. Train and test the algorithm on each subject within the non-amputee dataset, meaning the model is trained on 80% of the data from each non-amputee subject and then validated on the remaining 20% of the data from the same subject.
2. Train and test on each subject within the amputee data set, using the 80–20 data distribution, similar to the previous item.

3. Train and test the algorithm on each subject within the non-amputee dataset, meaning the model is trained on 50% of the data from each non-amputee subject and then validated on the remaining 50% of the data from the same subject.
4. Train and test on each subject within the amputee data set, using the 50–50 data distribution, similar to the previous item.
5. Train and test on the non-amputee dataset on a subject-independent basis, meaning the models are trained by using the data from all subjects except one in the non-amputee dataset.
6. Train and test on the amputee dataset with a subject-independent basis following the same paradigm as the previous step.
7. Test the effect of training with non-amputee data and testing on a single amputee subject.
8. Test the effect of training with non-amputee data and testing on the entire amputee dataset.
9. Evaluate the classification latency assessment of the system.

### 3. Results

This section systematically presents the findings from the experimental configurations delineated in Section 2. A granular analysis was performed, segregating the results based on two primary criteria: the source of the data—either from the non-amputee or the amputee cohorts—and the type of classification model employed—support vector machine (SVM) or long short-term memory (LSTM). This nuanced approach facilitates a comprehensive understanding of the relative performance and adaptability of the proposed models.

#### 3.1. Within-Subject Evaluation for Non-Amputee and Amputee Datasets

Each model—SVM and LSTM—was trained and tested intra-subject in two experimental scenarios. In the first scenario, for each subject, 80% of the available data were devoted to model training, while the remaining 20% were reserved for evaluation. In the second scenario, for each subject, 50% of the available data were allocated to model training, while the other 50% were reserved for evaluation. This experiment was conducted for both amputee and non-amputee datasets, with twenty non-amputee subjects and five amputee subjects. Four of the twenty-four non-amputee subjects initially evaluated were excluded due to irregularities identified during the data-review process.

The accuracy, precision, and F1 score were calculated for each model by five-fold cross-validation to ensure robustness and reliability. Table 3 shows the summary corresponding to the first distribution, 80–20. On the other hand, Table 4 shows the summary corresponding to the second distribution, 50–50.

The results corroborate that the SVM model tends to outperform the LSTM model across all the evaluated metrics—accuracy, precision, and F1 score—for both the amputee and non-amputee datasets. Likewise, the SVM is still shown to be superior at first glance in all the metrics evaluated in both the 80–20 and 50–50 distributions. Specifically, in the 80–20 distribution, the average accuracy of the SVM model on the amputee dataset was approximately 96.68%, compared to 93.39% for the LSTM model. Similar trends were observed with the non-amputee dataset, where the SVM model yielded an average accuracy of approximately 98.84%, in contrast to 93.36% for the LSTM model. Similarly, in the 50–50 distribution, the mean accuracy of the SVM model in the amputee dataset was approximately 95.35%, as opposed to 93.30% for the LSTM model. The mean accuracy of the SVM model on the non-amputee dataset was 95.46%, in contrast to 93.33% for the LSTM model. However, it was observed that the mean of the SVM metrics decreased and the standard deviation increased in the 50–50 distribution compared to the 80–20 distribution. This did not happen with the LSTM metrics, maintaining similar values in both distributions.

To enhance comprehension, Figure 8 illustrates bar plots representing the average performance metrics—accuracy, precision, and F1 score—across the two datasets, following the first 80–20 distribution. Figure 8a is dedicated to the non-amputee group, while

Figure 8b presents the results for the amputee group. Similarly, Figure 9 illustrates bar charts similar to those in Figure 8 but corresponding to the second 50–50 distribution.

**Table 3.** Summary of performance metrics for within-subject evaluation on amputee and non-amputee datasets using SVM and LSTM models and using the 80–20 data distribution.

Subject	Support Vector Machine			Long Short-Term Memory		
	Accuracy (%)	Precision (%)	F1 Score (%)	Accuracy (%)	Precision (%)	F1 Score (%)
Non-Amputee 01	99.20 ± 0.252	99.21 ± 0.240	99.21 ± 0.244	98.48 ± 0.202	98.39 ± 0.259	98.38 ± 0.187
Non-Amputee 02	97.70 ± 0.837	97.60 ± 0.760	97.22 ± 1.036	93.73 ± 0.518	92.91 ± 0.690	92.43 ± 0.587
Non-Amputee 03	97.94 ± 0.813	97.92 ± 0.898	97.92 ± 0.850	95.41 ± 0.538	95.48 ± 0.503	95.41 ± 0.524
Non-Amputee 04	96.82 ± 0.815	96.56 ± 0.919	96.46 ± 0.934	91.40 ± 0.732	91.11 ± 0.715	90.89 ± 0.791
Non-Amputee 05	97.02 ± 1.078	97.09 ± 1.018	97.00 ± 1.037	92.18 ± 0.911	92.31 ± 1.155	92.13 ± 0.916
Non-Amputee 06	94.63 ± 0.253	94.57 ± 0.282	94.34 ± 0.265	90.47 ± 0.945	90.50 ± 0.879	90.15 ± 1.010
Non-Amputee 07	97.69 ± 0.606	97.87 ± 0.501	97.70 ± 0.639	97.03 ± 0.279	96.94 ± 0.356	96.96 ± 0.278
Non-Amputee 08	96.76 ± 0.799	96.67 ± 0.863	96.11 ± 1.016	89.67 ± 0.493	88.00 ± 0.944	87.62 ± 0.719
Non-Amputee 09	96.40 ± 0.741	96.27 ± 0.782	96.18 ± 0.785	94.72 ± 0.482	94.40 ± 0.476	94.29 ± 0.529
Non-Amputee 10	96.41 ± 0.730	96.28 ± 0.719	95.94 ± 0.833	93.14 ± 0.676	93.10 ± 0.420	92.10 ± 0.821
Non-Amputee 11	96.01 ± 0.427	95.55 ± 0.512	95.34 ± 0.415	90.79 ± 0.520	90.37 ± 0.849	89.62 ± 0.480
Non-Amputee 12	97.90 ± 0.914	97.86 ± 0.869	97.51 ± 1.184	94.36 ± 0.660	93.35 ± 0.828	93.33 ± 0.889
Non-Amputee 13	95.97 ± 0.759	96.00 ± 0.743	95.73 ± 0.766	92.34 ± 0.463	91.63 ± 0.466	91.35 ± 0.609
Non-Amputee 14	97.51 ± 0.309	97.49 ± 0.325	97.37 ± 0.351	95.71 ± 0.696	95.27 ± 0.725	95.09 ± 0.795
Non-Amputee 15	96.62 ± 0.684	96.46 ± 0.745	96.40 ± 0.757	92.05 ± 0.588	91.94 ± 0.802	91.70 ± 0.585
Non-Amputee 16	96.77 ± 1.206	97.00 ± 1.156	96.68 ± 1.285	93.00 ± 0.846	93.30 ± 0.719	92.82 ± 0.930
Non-Amputee 17	95.11 ± 0.883	94.82 ± 0.843	94.66 ± 0.939	91.64 ± 0.605	90.49 ± 0.844	90.72 ± 0.719
Non-Amputee 18	96.17 ± 0.605	96.09 ± 0.627	95.65 ± 0.721	93.30 ± 0.470	93.41 ± 0.474	92.15 ± 0.629
Non-Amputee 19	97.34 ± 0.538	97.23 ± 0.578	96.79 ± 0.709	92.91 ± 0.358	92.36 ± 0.481	91.42 ± 0.401
Non-Amputee 20	96.90 ± 0.340	96.80 ± 0.388	96.71 ± 0.352	94.80 ± 0.434	94.87 ± 0.517	94.47 ± 0.454
<b>Non-Amputee Average</b>	<b>98.84 ± 0.679</b>	<b>96.77 ± 0.688</b>	<b>96.55 ± 0.756</b>	<b>93.36 ± 0.571</b>	<b>93.01 ± 0.655</b>	<b>92.65 ± 0.643</b>
Amputee 01	95.47 ± 0.869	95.46 ± 0.901	95.19 ± 0.985	91.38 ± 0.301	91.16 ± 0.445	90.87 ± 0.367
Amputee 02	95.31 ± 0.722	95.39 ± 0.700	95.31 ± 0.662	91.31 ± 0.494	91.25 ± 0.485	91.03 ± 0.436
Amputee 03	96.83 ± 0.532	97.18 ± 0.559	96.70 ± 0.591	94.33 ± 0.470	94.03 ± 0.629	93.96 ± 0.512
Amputee 04	97.05 ± 0.465	97.13 ± 0.506	96.98 ± 0.479	94.22 ± 0.299	94.36 ± 0.286	94.03 ± 0.315
Amputee 05	98.72 ± 0.447	98.67 ± 0.429	98.57 ± 0.436	95.69 ± 0.418	95.51 ± 0.414	95.47 ± 0.463
<b>Amputee Average</b>	<b>96.68 ± 0.607</b>	<b>96.77 ± 0.619</b>	<b>96.55 ± 0.631</b>	<b>93.39 ± 0.396</b>	<b>93.26 ± 0.452</b>	<b>93.07 ± 0.419</b>

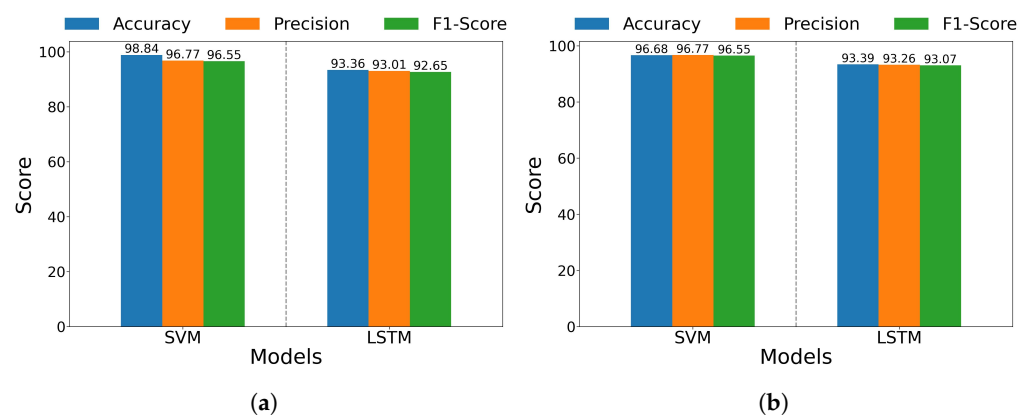


**Figure 8.** Bar plots for the average of performance metrics by using SVM and LSTM models in the 80–20 data distribution: (a) within-subject evaluation on non-amputee dataset, (b) within-subject evaluation on amputee dataset.

**Table 4.** Summary of performance metrics for within-subject evaluation on amputee and non-amputee datasets using SVM and LSTM models and using the 50–50 data distribution.

Subject	Support Vector Machine			Long Short-Term Memory		
	Accuracy (%)	Precision (%)	F1 Score (%)	Accuracy (%)	Precision (%)	F1 Score (%)
Non-Amputee 01	98.93 ± 0.423	98.96 ± 0.419	98.93 ± 0.433	98.17 ± 0.319	98.03 ± 0.336	98.04 ± 0.342
Non-Amputee 02	96.88 ± 0.673	96.64 ± 0.671	96.18 ± 0.733	93.66 ± 0.462	93.21 ± 0.478	92.32 ± 0.610
Non-Amputee 03	97.48 ± 1.428	97.49 ± 1.386	97.42 ± 1.459	95.37 ± 0.702	95.44 ± 0.640	95.36 ± 0.683
Non-Amputee 04	94.70 ± 1.371	94.24 ± 1.503	94.07 ± 1.493	91.91 ± 0.178	91.70 ± 0.258	91.41 ± 0.188
Non-Amputee 05	96.04 ± 0.781	96.20 ± 0.714	95.90 ± 0.818	91.94 ± 0.285	92.16 ± 0.370	91.91 ± 0.285
Non-Amputee 06	91.69 ± 1.379	91.69 ± 1.481	91.21 ± 1.364	89.93 ± 0.470	89.94 ± 0.647	89.57 ± 0.481
Non-Amputee 07	96.48 ± 0.812	96.78 ± 0.894	96.42 ± 0.928	96.63 ± 0.398	96.53 ± 0.400	96.56 ± 0.399
Non-Amputee 08	94.44 ± 1.223	94.20 ± 1.164	93.13 ± 1.640	88.57 ± 0.612	87.52 ± 0.664	85.99 ± 0.961
Non-Amputee 09	95.32 ± 0.935	95.17 ± 0.892	94.97 ± 1.025	94.91 ± 0.161	94.68 ± 0.117	94.47 ± 0.190
Non-Amputee 10	95.24 ± 0.734	95.05 ± 0.632	94.53 ± 0.799	93.83 ± 0.783	93.58 ± 0.660	92.95 ± 0.919
Non-Amputee 11	93.48 ± 1.463	92.90 ± 2.043	92.34 ± 1.828	91.31 ± 0.752	90.61 ± 0.744	90.20 ± 0.876
Non-Amputee 12	97.25 ± 1.248	97.09 ± 1.317	96.65 ± 1.567	95.40 ± 0.744	94.89 ± 0.762	94.72 ± 0.933
Non-Amputee 13	94.36 ± 1.058	94.14 ± 1.294	93.76 ± 1.266	92.52 ± 0.421	91.99 ± 0.320	91.70 ± 0.498
Non-Amputee 14	95.93 ± 0.683	95.90 ± 0.694	95.62 ± 0.765	95.65 ± 0.528	95.21 ± 0.500	95.11 ± 0.512
Non-Amputee 15	95.73 ± 0.861	95.47 ± 0.890	95.42 ± 0.920	91.89 ± 0.774	91.69 ± 0.951	91.60 ± 0.868
Non-Amputee 16	94.65 ± 1.318	94.87 ± 1.256	94.30 ± 1.510	92.98 ± 0.969	92.98 ± 1.183	92.86 ± 0.950
Non-Amputee 17	94.19 ± 1.239	94.20 ± 1.291	93.56 ± 1.493	91.01 ± 0.542	89.75 ± 0.701	89.92 ± 0.604
Non-Amputee 18	94.82 ± 0.712	94.72 ± 0.865	94.05 ± 0.757	93.39 ± 0.321	93.03 ± 0.430	92.11 ± 0.271
Non-Amputee 19	95.88 ± 0.579	95.74 ± 0.659	95.00 ± 0.688	92.63 ± 0.725	91.75 ± 0.752	91.23 ± 0.757
Non-Amputee 20	95.80 ± 0.967	95.60 ± 1.025	95.42 ± 1.049	94.94 ± 0.641	94.98 ± 0.596	94.61 ± 0.702
<b>Non-Amputee Average</b>	<b>95.46 ± 0.994</b>	<b>95.35 ± 1.055</b>	<b>94.94 ± 1.127</b>	<b>93.33 ± 0.539</b>	<b>92.98 ± 0.575</b>	<b>92.63 ± 0.601</b>
Amputee 01	93.85 ± 2.275	94.07 ± 2.150	93.50 ± 2.489	91.41 ± 0.929	91.21 ± 1.024	90.98 ± 1.010
Amputee 02	93.58 ± 1.121	93.77 ± 1.228	93.70 ± 1.048	90.82 ± 0.618	90.89 ± 0.687	90.59 ± 0.632
Amputee 03	95.84 ± 1.300	96.34 ± 1.016	95.52 ± 1.486	94.47 ± 0.249	94.17 ± 0.326	94.06 ± 0.278
Amputee 04	95.82 ± 0.264	95.96 ± 0.346	95.72 ± 0.265	94.18 ± 0.641	94.25 ± 0.789	94.04 ± 0.689
Amputee 05	97.67 ± 1.058	97.61 ± 1.075	97.45 ± 1.107	95.63 ± 0.530	95.48 ± 0.543	95.37 ± 0.531
<b>Amputee Average</b>	<b>95.35 ± 1.204</b>	<b>95.55 ± 1.163</b>	<b>95.18 ± 1.279</b>	<b>93.30 ± 0.593</b>	<b>93.20 ± 0.674</b>	<b>93.01 ± 0.628</b>

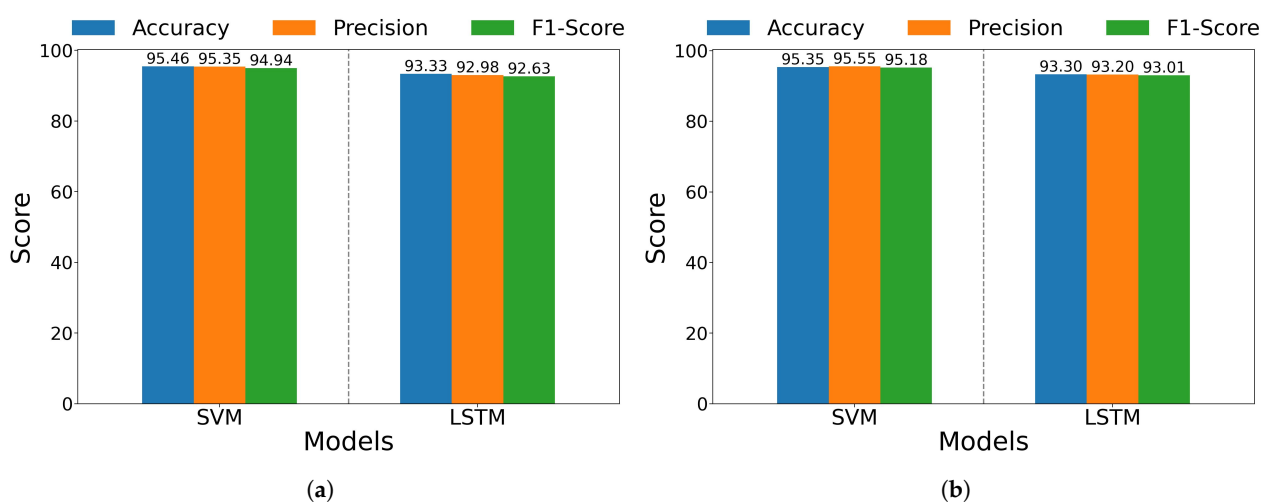


**Figure 9.** Bar plots for the average of performance metrics by using SVM and LSTM models in the 50–50 data distribution: (a) within-subject evaluation on non-amputee dataset, (b) within-subject evaluation on amputee dataset.

Before conducting the principal analysis, the normality of the data and the homogeneity of variances, which are crucial prerequisites for ANOVAs, were assessed. The Shapiro–Wilk test confirmed the normality of the performance metrics (accuracy, precision,

and F1 score) for both the SVM and LSTM models across different scenarios ( $p > 0.05$  in all cases), suggesting that the data were normally distributed. Additionally, Levene's test for the homogeneity of variances showed no significant differences between the groups ( $p > 0.05$  for all metrics), satisfying the assumption of the homogeneity of variances.

A two-way ANOVA was conducted to investigate the effects of the 'Model Type' (SVM vs. LSTM) and 'Training/Testing Split' (80–20 vs. 50–50) on the performance metrics. The analysis revealed that the 'Model Type' significantly affected the accuracy ( $F(1, 116) = 54.61, p < 0.0001$ ), precision ( $F(1, 116) = 62.55, p < 0.0001$ ), and F1 score ( $F(1, 116) = 54.14, p < 0.0001$ ). However, the 'Training/Testing Split' and the interaction between the 'Model Type' and 'Training/Testing Split' did not significantly affect these metrics ( $p > 0.05$  for all).

Following the significant findings from the ANOVA, Tukey's HSD post hoc test was conducted to determine specific pairwise differences between the SVM and LSTM models. The results indicated significant differences in all the performance metrics, further substantiating the superior performance of the SVM model over the LSTM model in this context.

### 3.2. Cross-Subject Evaluation on Non-Amputee Dataset and Amputee Dataset

To evaluate the generalizability of the support vector machine (SVM) and long short-term memory (LSTM) models, a leave-one-out cross-validation (LOOCV) methodology was utilized. Each iteration of this approach's model training and testing cycle excludes one subject. The training set contains the remaining subjects, with 20% of the data used as a validation set. Figure 10 offers a schematic representation of this data-partitioning strategy.

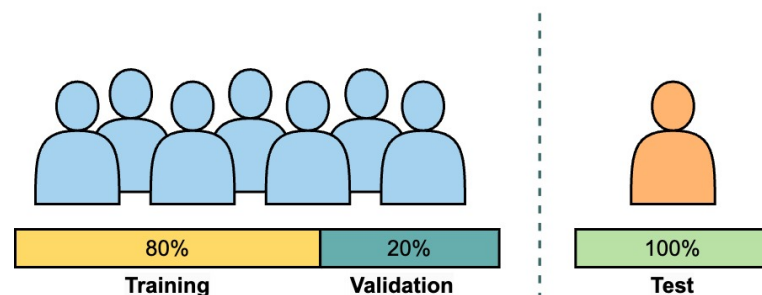


**Figure 10.** Schematic representation of data partitioning in LOOCV strategy.

After the initial evaluation, the model is subjected to domain-adaptation techniques. The correlation alignment (CORAL) method was used for models involving SVM. The transfer learning technique was used for LSTM models. This iterative procedure was carried out until each subject was singularly excluded from the training set and used for testing. Performance metrics were calculated before and after applying domain-adaptation techniques for the amputee and non-amputee datasets. Notably, domain-adaptation techniques led to significant enhancements, particularly in the LSTM model. For example, while the accuracy of the SVM model improved from 49.52% to 53.22%, the accuracy of the LSTM model improved from 46.16% to 71.86% with the amputee dataset.

Figure 11 further illustrates the comparative performance of the models before and after the application of domain-adaptation techniques. These metrics and other performance measures are comprehensively detailed in Table 5.

**Table 5.** Average performance metrics of SVM and LSTM models before and after applying domain-adaptation techniques on amputee and non-amputee datasets.

Group Subject		Support Vector Machine			Long Short-Term Memory		
		Accuracy(%)	Precision (%)	F1 Score (%)	Accuracy(%)	Precision (%)	F1 Score (%)
Amputee Group	Before	49.52 ± 6.06	47.33 ± 6.75	48.61 ± 5.48	46.16 ± 7.69	44.21 ± 7.92	47.22 ± 6.63
	After	53.22 ± 6.22	48.84 ± 6.65	49.68 ± 5.02	71.86 ± 0.67	69.83 ± 1.61	72.00 ± 2.19
Non-amputee Group	Before	68.45 ± 7.59	64.13 ± 8.33	66.57 ± 6.26	67.22 ± 8.16	63.67 ± 7.90	65.52 ± 6.64
	After	70.37 ± 7.38	64.83 ± 8.10	68.52 ± 5.94	90.37 ± 0.18	89.45 ± 0.75	90.36 ± 1.03

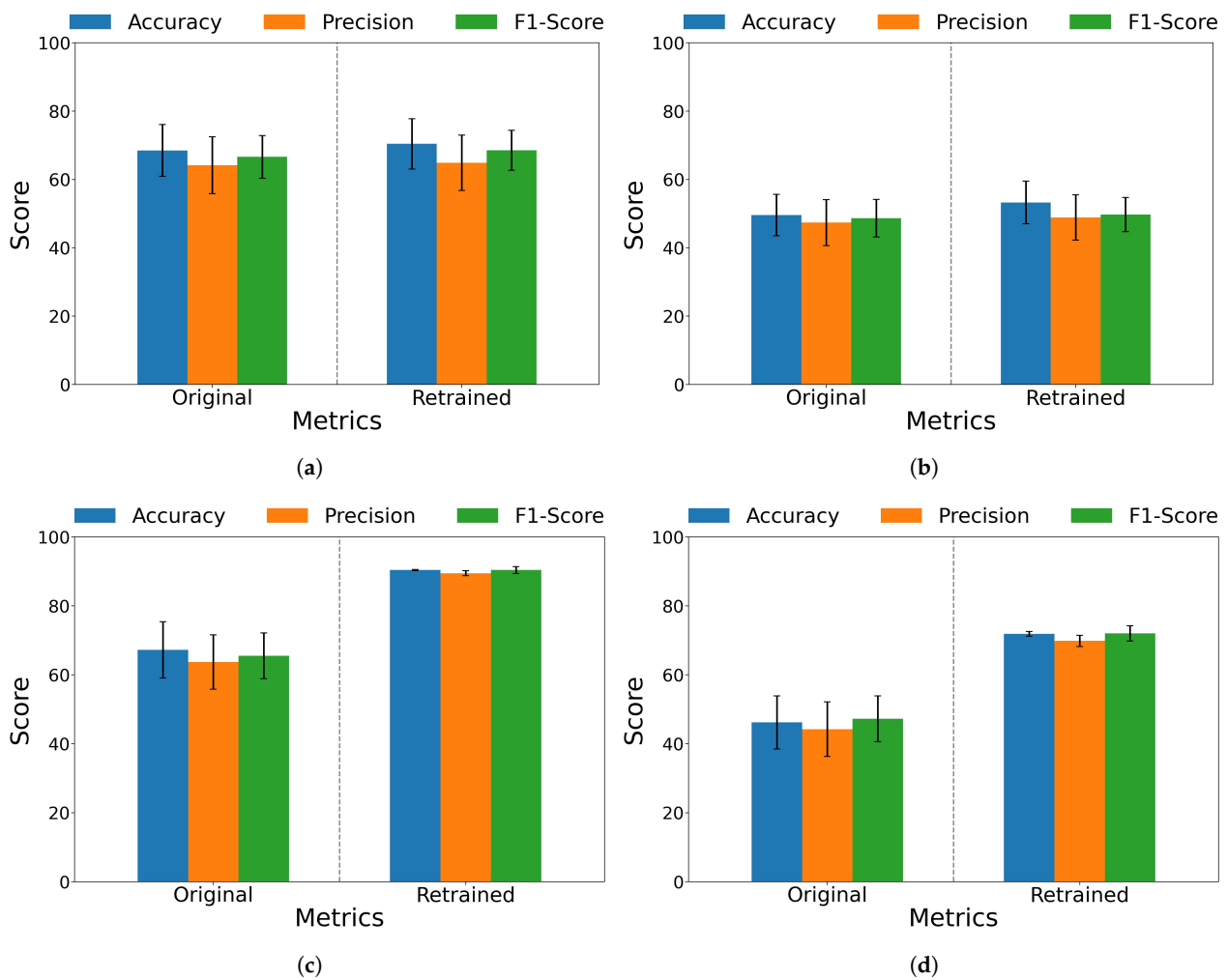


**Figure 11.** Comparative performance metrics of SVM and LSTM models before and after applying domain-adaptation techniques across non-amputee and amputee datasets. (a) SVM performance on non-amputee dataset. (b) SVM performance on amputee dataset. (c) LSTM performance on non-amputee dataset. (d) LSTM performance on amputee dataset.

After the comparative performance analysis, Figure 12 provides confusion matrices for the SVM and LSTM models after applying their corresponding domain-adaptation technique. These matrices are shown for both the non-amputee and amputee datasets. Including the confusion matrices allows for a more nuanced interpretation of the classification performance, specifically detailing true positives, true negatives, false positives, and false negatives.

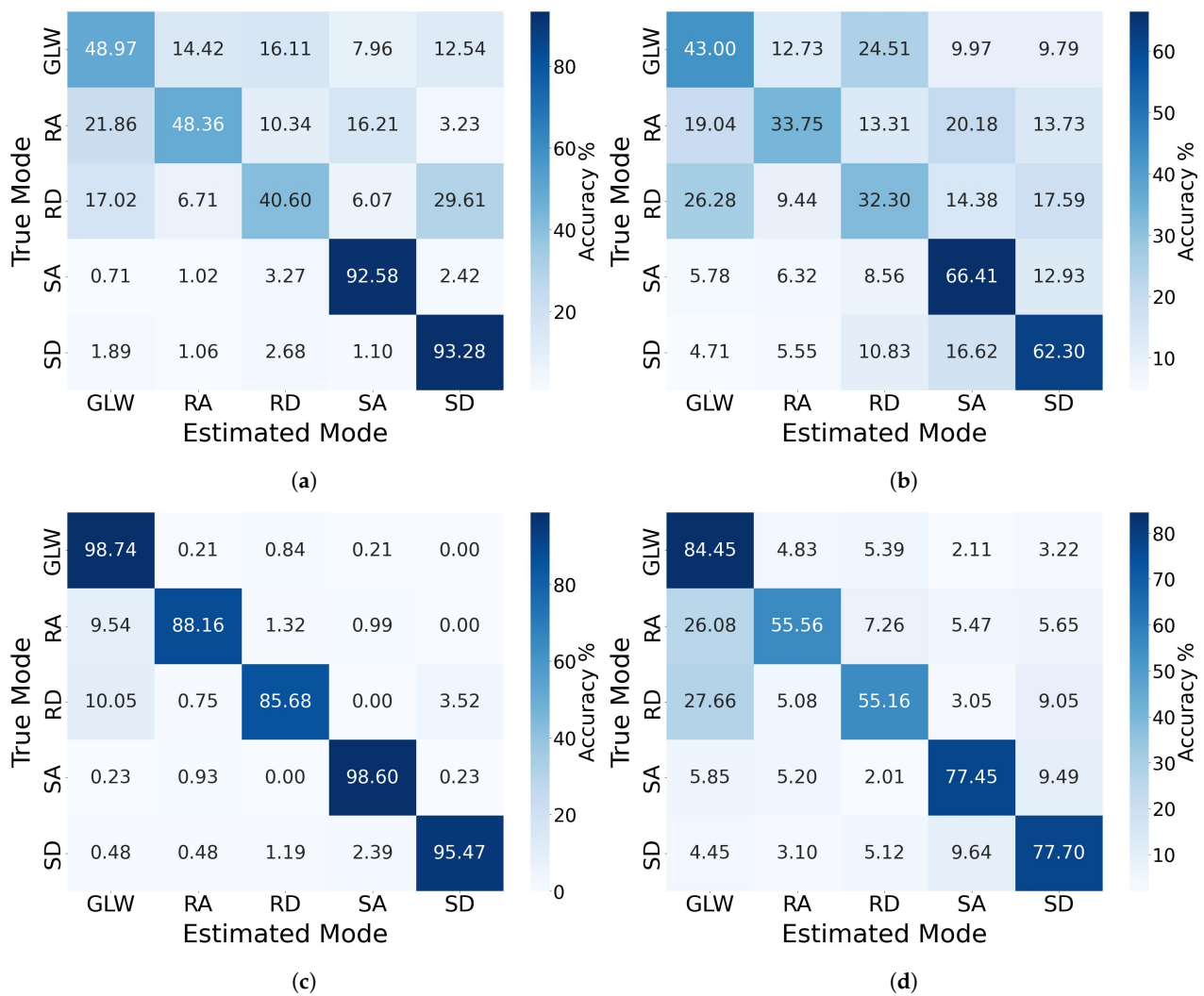


**Figure 12.** Confusion matrices of SVM and LSTM models with domain-adaptation techniques across non-amputee and amputee datasets. (a) SVM model on the non-amputee dataset, (b) SVM model on the amputee dataset, (c) LSTM model on the non-amputee dataset, and (d) LSTM model on the amputee dataset.

A repeated-measures ANOVA was employed to analyze the effects of the model type (SVM vs. LSTM), domain-adaptation status (before vs. after), and subject type (amputee vs. healthy) on the performance metrics: accuracy, precision, and F1 score. The analysis revealed several key findings. For accuracy, the effects of the model type were significant ( $F(1, 16) = 6.51, p = 0.0214$ ), as well as the effects of domain adaptation ( $F(1, 16) = 13.96, p = 0.0018$ ) and subject type ( $F(1, 16) = 41.35, p < 0.0001$ ). There was also a significant interaction between model type and domain adaptation ( $F(1, 16) = 14.69, p = 0.0015$ ). Similar patterns were observed for the precision and F1 score, with significant effects for model type (precision:  $F(1, 16) = 14.10, p = 0.0017$ ; F1 score:  $F(1, 16) = 8.46, p = 0.0103$ ), domain adaptation (precision:  $F(1, 16) = 23.56, p < 0.0002$ ; F1 score:  $F(1, 16) = 14.89, p = 0.0014$ ), and subject type (precision:  $F(1, 16) = 60.02, p < 0.0001$ ; F1 score:  $F(1, 16) = 37.41, p < 0.0001$ ). The interaction effects between model type and domain adaptation were also significant across these metrics.

From this experiment, it can be concluded that the LSTM model emerged as particularly robust, displaying superior performance metrics with lower variability after the application of domain-adaptation techniques. The results underscore the potential of LSTM models in this application and indicate avenues for future research, especially concerning the amputee dataset.

### 3.3. Inter-Population Generalizability

The objective of this experiment is to assess the ability of the classifiers to generalize across populations. The 20 non-amputee subjects were divided into two subgroups: 15 for model training and 5 for testing. Two different test scenarios were considered, one with a single amputee subject and the other test with all five amputee subjects.

After the initial testing phase, each model was subjected to domain-adaptation techniques. The correlation alignment (CORAL) technique was used for the SVM models, and the transfer learning technique was used for the LSTM models. These techniques were applied to explore their effects on generalizability across populations.

In the first scenario summarized in Table 6, the initial F1 scores of the SVM and LSTM models were 42.73% and 45.86%, respectively. After applying domain-adaptation techniques, the SVM model obtained a slight performance improvement, raising its F1 score to 45.32%. However, the LSTM model obtained a substantial performance improvement, raising its F1 score to 72.75%.

**Table 6.** Performance metrics of SVM and LSTM models using a 15-subject non-amputee training set, with and without domain-adaptation techniques on a single amputee subject.

	Support Vector Machine			Long Short-Term Memory		
	Accuracy (%)	Precision (%)	F1 Score (%)	Accuracy (%)	Precision (%)	F1 Score (%)
Before	43.14	43.04	42.73	45.86	45.81	45.68
After	45.71	45.83	45.32	73.07	76.16	72.75

As summarized in Table 7, the initial F1 scores of the SVM and LSTM models in the second scenario were 43.07% and 44.30%, respectively. After applying domain-adaptation techniques, the SVM model obtained a slight performance improvement, raising its F1 score to 44.02%. However, the LSTM model improved substantially, raising its F1 score to 69.30%.

**Table 7.** Performance metrics of SVM and LSTM models using a 15-subject non-amputee training set, with and without domain-adaptation techniques on multiple amputee subjects.

	Support Vector Machine			Long Short-Term Memory		
	Accuracy (%)	Precision (%)	F1 Score (%)	Accuracy (%)	Precision (%)	F1 Score (%)
Before	43.60	43.82	43.07	45.21	46.38	44.30
After	44.23	43.94	44.02	70.57	71.81	69.30

After applying domain-adaptation techniques, the results obtained in the second scenario, in general, showed that the techniques slightly decreased their performance on all metrics compared to the results for the first scenario. The LSTM models consistently demonstrated a higher accuracy than the SVM models, with a relatively high difference of at least 25 points. These results suggest that the LSTM model is more robust and has a higher capacity for inter-population generalizability.

Although both models experienced improvements in their performance after the application of domain-adaptation techniques, the metrics obtained did not reach the expected level. This limitation could be attributed to the complexity of the dataset, which incorporates approximately 50 features per sample. These numerous and diverse features imply that the signals are inherently different, making it difficult for a preset algorithm to adapt efficiently to a new individual or amputee. In this context, the intrinsic complexity of the dataset emerges as a significant challenge, hindering the ability of models to achieve an optimal performance in adapting to specific situations.

### 3.4. Classification Latency Assessment

One of the critical factors in real-time classification tasks is the system's response time, often called the "classification latency". The latency was evaluated for both the SVM and LSTM models, encompassing the amputee and healthy-subject datasets. Table 8 summarizes the average classification latency for the SVM and LSTM models. The average latency for the SVM model was 19.84 ms, while it was 37.07 ms for the LSTM model. These latency times are well within the overlapping window time of 40 ms and acceptable limits for real-time applications of 300 ms [14], thereby demonstrating the practicality of the proposed models for real-world implementations.

**Table 8.** Classification running time of SVM and LSTM models.

Model	Average Latency (ms)
Support Vector Machine	19.84
Long Short-Term Memory	37.07

## 4. Discussion

### 4.1. Locomotion Modes

Undertaking a chronological exploration of the presented studies, several salient points emerge, as shown in Table 9.

**Table 9.** Comparison between this research and previous research regarding classification of locomotion modes acquired with EMG and IMU signals.

Author/Year	Muscle	Locomotion Modes	Participants	Accuracy
Miller et al., 2013 [6]	Tibialis anterior, medial gastrocnemius, vastus lateralis, biceps femoris	Ground-level walking, ramp ascent, ramp descent, stairs ascent, stairs descent	5 non-amputees, 5 transtibial amputees	94.7%, 97.9%
Meng et al., 2021 [17]	Rectus femoris, vastus lateralis, biceps femoris, semitendinosus, tibialis anterior, medial gastrocnemius, lateral gastrocnemius	Ground-level walking, ramp ascent, ramp descent, stairs ascent, stairs descent, standing, sitting	10 non-amputees	98.0%
Barberi et al., 2023 [15]	Adductor longus, rectus femoris, biceps femoris, tensor fasciae latae	Ground-level walking, ramp ascent, ramp descent, stairs ascent, stairs descent	13 transfemoral amputees	94.0%
Present study	Adductor longus, rectus femoris, biceps femoris, tensor fasciae latae	Ground-level walking, ramp ascent, ramp descent, stairs ascent, stairs descent	20 non-amputees, 5 transtibial amputees	98.8%, 96.7%

Commencing with Miller et al.'s research in 2013 [6], there is an evident reliance on a blend of muscles from the upper and lower extremities for electromyography (EMG) data acquisition. Predominantly, the tibialis anterior and the medial gastrocnemius were pivotal muscles in their investigation. Notably, their cohort included an amalgamation of non-amputees and transtibial amputees, and the range of locomotion modes spanned from rudimentary ground-level walking to the more complex tasks of stair navigation. Yet, in the face of this heterogeneity, the research yielded substantial accuracy rates of 94.7% for non-amputees and 97.9% for transtibial amputees.

The subsequent year, 2021, saw Meng et al. [17] embark on an extensive muscle-selection protocol, garnering data from seven muscles. Their inclusion criteria for muscles ensured representation from both the upper- and lower-leg regions. What distinguished their study was the incorporation of static postures, notably standing and sitting, alongside other locomotion modes. With this exhaustive approach, they secured an accuracy pinnacle of 98% among the non-amputee cohort.

Transitioning to Barberi et al.'s 2023 study [15], there was a palpable shift towards an emphasis on proximal muscles of the thigh, incorporating muscles such as the adductor longus and the rectus femoris. Solely focusing on transfemoral amputees, their endeavors culminated in a respectable accuracy rate of 94%. Our current study, however, echoing a similar muscle preference, cast a broader net regarding participant inclusion, embracing both non-amputees and transtibial amputees. The accuracy metrics remain commendable, standing at 98.8% for non-amputees and 96.7% for transtibial amputees.

#### 4.2. Relevance of Electromyography (EMG), Inertial Measurement Units (IMU), and Data Fusion

Electromyography (EMG) can detect the intention of movement even before the physical action occurs. EMG signals have demonstrated their significance in predicting human movement intent [29], offering valuable insight into pre-action planning. In parallel, inertial measurement units (IMU) provide the ability to segment data; identify gait cycles; and potentially, in future work, identify specific phases within the gait cycle [30]. IMU data segmentation and analysis contribute to a more complete understanding of motion patterns and gait dynamics. Notably, given the individual variations in gait patterns among participants, a typical pattern was discovered in the Z acceleration of the tibia and foot. This specific pattern enabled us to identify the gait cycles and played a pivotal role in effectively segmenting the data.

The combination of the EMG and IMU signals approach leverages the strengths of each sensor, leading to the more appropriate and precise classification of locomotion tasks. Data fusion enhances the overall performance of locomotion task classification [31], offering a comprehensive perspective on human movement intent and gait dynamics. This integrated approach allows for a deeper understanding of the complexities of locomotion, potentially advancing research and practical applications. A noteworthy aspect is that the fusion of EMG and IMU data in this study enhanced the model's performance and contributed to its robustness across different locomotion tasks. Combining these two data types captures a broader spectrum of biomechanical and physiological characteristics, thereby improving the classifier's ability to distinguish between complex locomotion tasks. This is especially evident in the results, where enhanced performance metrics were observed compared to studies that utilized either EMG or IMU data in isolation.

#### 4.3. Sensors Positioning

Four thigh muscles were selected for data collection—rectus femoris, biceps femoris, adductor, and tensor fasciae latae—for the strategic placement of EMG sensors. The experimental positioning identified critical factors impacting the quality of EMG signals. The presence of vellus hair on the thigh posed a challenge by impeding sensor adherence to the skin, inducing relative movement between the sensor and the user's muscle. Another factor that positively influenced the signal quality was the alignment of the sensors with the orientation of muscle fibers, resulting in a notably sharper signal and better tolerance to noise [32].

Muscle selection was guided by the practicality of the sensor application, considering that in developing countries, most individuals with transtibial amputations use sockets that cover a significant portion of the stump, including the knee region. The raw EMG data analysis revealed myoelectric variations among muscles during locomotion tasks, highlighting the rectus femoris as a critical flexor muscle with greater amplitude. Furthermore, depending on the intended locomotion activity, the signals acquired by EMG exhibited variations in amplitude and latency attributed to the effort and duration required for each activity. For instance, the activity of stairs descent displayed greater amplitude in its EMG signals than ramp descent, serving as a distinguishing factor between these two activities.

#### 4.4. Architectures of the Algorithms

The growing development of machine learning has encouraged various studies to take the opportunity to develop more suitable algorithms for the lower-limb prosthesis control

system. The studies presented in Table 10 used machine learning to classify aspects related to the control of lower-limb prosthesis.

**Table 10.** Comparison between this research and previous research regarding the architecture of algorithms using different machine learning methods.

Author/Year	Dataset	Data Acquisition	Architectures of the Algorithms	Machine Learning Method	Accuracy
Bruinsma et al., 2021 [33]	Transfemoral amputee	IMU	RNNs + 4 × GRU + 2 × dense layers	LDA	93.0%
			RNNs + 4 × LSTM + 2 × dense layers	LDA	90.0%
Zhou et al., 2021 [16]	Ankle-foot motion	EMG + IMU	BiLSTM layer + dense layer + Softmax	BiLSTM	99.8%
				SVM	90.4%
				ANN	94.7%
				Decision tree (DT)	74.5%
				Naive Bayes (NB)	82.5%
Mazon et al., 2022 [14]	Transfemoral amputee	IMU	2 × ReLU + Dropout + 2 × dense layer + Softmax	LSTM	95.0%
Putri et al., 2023 [34]	Transtibial amputee	EMG	Hidden	ANN	96.0%
Present study	Transtibial amputees	EMG + IMU	Lineal kernel, 2nd order poly kernel	SVM	98.8%
			BiLSTM + Dropout + BiLSTM + Dropout + ReLU + Softmax	LSTM	93.4%

The research by Bruinsma et al. [33] in 2021 encompasses a dataset from one osseointegrated transfemoral amputee for the acquisition of only inertial data (IMU). What distinguished their study was the use of the machine learning method LDA with three deep neural network architectures in their research (CNNs, RNNs, and CRNNs). The analysis showed an accuracy rate of 90% for LSTM and 93% for the GRU. Among the multiple architectures analyzed, the best performance was the GRU (Gated Recurrent Unit) in combination with RNNs (recurrent neural networks).

Zhou et al. [16], months later, conducted tests with different machine learning algorithms to classify ankle movements. The algorithms used included Naive Bayes (NB), decision tree (DT), artificial neural networks (ANNs), support vector machine (SVM), and bi-directional long short-term memory (BiLSTM). Their dataset consisted of EMG and inertial signals from three non-amputee subjects. Their study confirmed the effectiveness of the SVM and BiLSTM algorithms, achieving accuracies of 90.8% and 99.8%, respectively.

In the following year, 2022, Mazon et al. [14] focused on classifying locomotion modes, obtaining data from one osseointegrated transfemoral amputee by using only inertial data. They focused on using two types of architecture: a convolutional neural network and convolutional recurrent neural network CNN-(LSTM/GRU). Noteworthy, they achieved a peak accuracy of 95% with a system composed of CNN-LSTM networks, which can correctly classify data for the transfemoral amputee subject.

Moving on to Putri et al.'s [34] study in 2023, there was a palpable shift, solely focusing on using an ANN (artificial neural network) as a machine learning method. They used EMGs for data acquisition with a respectable precision rate of 96%. However, the architecture used for development was still being determined.

The studies presented above used different algorithms, among which SVM and LSTM stand out. However, these algorithms have been used to classify ankle movements, gait

cycle phases, or locomotion activities in non-amputees. In contrast to past studies, in this research, the two most prominent algorithms, SVM and LSTM, are used to classify locomotion activities in both non-amputees and transtibial amputees by using EMG and IMU data fusion. In addition, the generalizability of both algorithms was explored to evaluate the ability to classify amputee locomotion tasks with algorithms trained on non-amputee data.

#### *4.5. Dataset Composition and Its Implications*

One of the significant strengths of this study lies in the composition of the dataset, which includes data from twenty non-amputated individuals and five transtibial amputees. This diverse dataset enabled a multi-faceted evaluation in three critical dimensions: a within-subject evaluation, cross-subject evaluation within each dataset, and inter-dataset evaluation.

The inclusion of a reasonable number of subjects in both the amputee and non-amputee cohorts allowed for a rigorous assessment of the performance of the models on an intra-subject basis, in addition to facilitating a cross-subject analysis, thereby addressing the generalizability of the classifiers within the same population. The juxtaposition of the amputee and non-amputee data made it feasible to conduct experiments scrutinizing the model's adaptability across different populations. This is critical in real-world applications where a model trained on one demographic must often be generalized to another. Such a comprehensive analysis was only possible with a more diverse or smaller dataset.

A significant focal point of this study was to assess the generalizability of models trained on non-amputee data when applied to amputee subjects. The results affirm that while the models can adapt to new data types through retraining, the performance remains suboptimal compared to that achieved on non-amputee subjects. This draws attention to the need to develop specialized algorithms or incorporate additional features to enhance model adaptability across heterogeneous populations.

#### *4.6. Domain-Adaptation in SVM and LSTM Models*

Domain-adaptation techniques were implemented for SVM and LSTM models to enhance the classification of locomotion tasks in transtibial amputees by using EMG and IMU data. For the SVM models, the CORAL method was applied to align the feature distributions of the source and target domains by matching their covariances. This approach, however, yielded mixed results in terms of performance metrics, prompting the consideration of alternative methods like coupled SVMs for a more nuanced approach to non-linear discrepancies in the data. On the other hand, transfer learning was applied with LSTM models, demonstrating a significant increase in the performance metrics and a reduction in their standard deviation. This highlights the effectiveness of transfer learning in capturing the temporal and complex patterns in the data, which may need to be fully addressed by the CORAL method in SVM models.

Incorporating transfer learning with LSTM models in this study was instrumental in addressing the challenges posed by the locomotion data's high-dimensional and non-linear nature. Unlike CORAL's relatively modest impact on SVM model performance, transfer learning in LSTMs showed a robust improvement in classification accuracy and consistency, underscoring its suitability for complex data types. This comparative effectiveness emphasizes the need for a multifaceted approach to domain adaptation, where different techniques are optimized for specific model architectures and data characteristics. The findings suggest that while methods like CORAL can offer computational efficiency in SVM models, integrating transfer learning with LSTM models provides a more comprehensive solution for enhancing the classification of locomotion tasks in transtibial amputees, warranting further exploration in future studies.

#### 4.7. Limitations and Future Outlook

This study has made noteworthy contributions to the classification of locomotion tasks for both transtibial amputees and non-amputees. However, addressing the computational aspects associated with the LSTM and SVM models is crucial. While the SVM model showed a better generalization performance, the computational expenses of extracting features from EMG and IMU signals for real-time operation in embedded systems should be addressed. Although both models achieved classification times under 40 ms—matching the overlapping window duration—this does not account for the time required for feature extraction. Optimizing feature extraction and classification algorithms for a lower computational overhead will be essential for real-world deployments.

Likewise, concerning hardware aspects, it was observed that four EMG sensors and three IMU sensors were sufficient to collect representative data, enabling the differentiation of five locomotion tasks. Noteworthy, the sensors used in data collection, DELSYS Trigno Avanti, are high-end. For future research, exploring the possibility of using low-cost sensors for prosthetic control could make them more accessible, especially in developing countries.

Regarding prosthetic sensor placement, the need for expert intervention and the potential user discomfort associated with locating and attaching sensors for each use present practical challenges. Future endeavors should explore cost-effective sensor solutions with an efficient and user-friendly configuration.

Moreover, prospective research should focus on integrating EMG sensors into customized prosthetic sockets in predetermined positions. This integrated sensor design implemented with the classification algorithm in the control system of a lower-limb prosthesis based on data fusion (EMG + IMU) would have the potential to detect movement intentions more swiftly and accurately without requiring sensor adaptations by experts or causing discomfort for users. This approach enhances the user experience and offers a promising avenue for future investigations in prosthetic technology.

From a clinical standpoint, the utility of the proposed models hinges on their ability to generalize well to real-world, diverse patient populations. Future work should focus on clinically validating these models in various settings and possibly integrating them into prosthetic devices to assess their utility in real-time, dynamic environments.

#### 5. Conclusions

This paper presents a methodology for data acquisition through EMG and IMU sensors, testing both non-amputees and transtibial amputees. A marked differentiator was identified in the raw EMG data from the four thigh muscles tested, allowing for the successful classification of five locomotion tasks. A comparative analysis between the SVM and LSTM models for task classification revealed that the fusion of EMG and IMU signals substantially improved the classification accuracy, supporting the efficacy of multimodal data in locomotion task recognition.

The results of the first comparison highlighted a superior performance of the SVM model in task classification in individual assessments of transtibial amputee and non-amputee subjects. However, after implementing domain-adaptation techniques, subsequent comparisons revealed that the LSTM model exhibits greater robustness and a better intra-population and inter-population generalization ability. Both models demonstrated acceptable latency times, meeting the established real-time requirements, thus highlighting their potential application in embedded systems and real-time environments.

For future research, it is suggested to focus efforts towards integrating EMG and IMU sensors directly into the prosthetic socket, thus enabling their functionality in a more integrated manner. The effective generalization of classification models becomes crucial in this context as it facilitates successfully incorporating these devices in dynamic and real-time environments, thus enhancing their practical utility and clinical applicability.

**Author Contributions:** Conceptualization, V.E.A., G.O., O.A.G.-H. and D.A.E.; methodology, V.E.A., G.O. and O.A.G.-H.; software, O.A.G.-H.; validation, V.E.A., G.O., O.A.G.-H., D.A.E. and J.G.C.-E.; formal analysis, O.A.G.-H.; investigation, G.O., J.G.C.-E. and V.E.A.; resources, V.E.A. and D.A.E.; data curation, G.O.; writing—original draft preparation, G.O., O.A.G.-H., J.G.C.-E. and V.E.A.; writing—review and editing, G.O., O.A.G.-H., J.G.C.-E., V.E.A. and D.A.E.; visualization, G.O., O.A.G.-H. and J.G.C.-E.; supervision, V.E.A. and D.A.E.; project administration, V.E.A. and D.A.E.; funding acquisition, D.A.E. All authors have read and agreed to the published version of the manuscript.

**Funding:** This research was funded by “Programa Piloto de proyectos de Investigación en áreas transversales en el Departamento de Ingeniería de la Pontificia Universidad Católica del Perú”, grant number FGR-2023.

**Institutional Review Board Statement:** This study was conducted in accordance with the Declaration of Helsinki and was approved by the Ethics Committee for Research in Life Sciences and Technologies of Pontificia Universidad Católica del Perú (protocol code: N°073-2023-CEICVyT/PUCP; date of approval: 21 August 2023).

**Informed Consent Statement:** Informed consent was obtained from all the subjects involved in this study.

**Data Availability Statement:** Data are contained within the article.

**Conflicts of Interest:** The authors declare no conflict of interest.

## Abbreviations

The following abbreviations are used in this manuscript:

ANOVA	Analysis of variance
AL	Adductor longus
BF	Biceps femoris
Bi-LSTM	Bi-directional long short-term memory
CORAL	Correlation alignment
EMG	Electromyographic
FT	Foot
GLW	Ground-level walking
HSD	Honest significant difference
IMU	Inertial measurement unit
LOOCV	Leave-one-out cross-validation
LSTM	Long short-term memory
RBF	Radial basis function
RPA	Ramp ascent
RPD	Ramp descent
RF	Rectus femoris
SSA	Stairs ascent
SSD	Stairs descent
SVM	Support vector machine
TF	Tensor fasciae latae
TB	Tibia

## References

- Vázquez, E. *Los Amputados y su Rehabilitación. Un Reto Para el Estado*; Intersistemas: Ciudad de México (CDMX), Mexico, 2016; p. 5.
- Ziegler-Graham, K.; MacKenzie, E.J.; Ephraim, P.L.; Travison, T.G.; Brookmeyer, R. Estimating the prevalence of limb loss in the united states: 2005 to 2050. *Arch. Phys. Med. Rehabil.* **2008**, *89*, 422–429. [[CrossRef](#)]
- Molina, C.S.; Faulk, J. *Lower Extremity Amputation*; StatPearls Publishing: Treasure Island, FL, USA, 2022.
- Su, B.-Y.; Wang, J.; Liu, S.-Q.; Sheng, M.; Jiang, J.; Xiang, K. A CNN-based method for intent recognition using inertial measurement units and intelligent lower limb prosthesis. *IEEE Trans. Neural Syst. Rehabil. Eng.* **2019**, *27*, 1032–1042. [[CrossRef](#)]
- Farro, L.; Tapia, R.; Bautista, L.; Montalvo, R.; Iriartem, H. Características clínicas y demográficas del paciente amputado. *Rev. Med. Hered.* **2012**, *23*, 240–243. [[CrossRef](#)]
- Miller, J.D.; Beazer, M.S.; Hahn, M.E. Myoelectric walking mode classification for transtibial amputees. *IEEE Trans. Biomed. Eng.* **2013**, *60*, 2745–2750. [[CrossRef](#)]

7. Sherrat, F.; Plummer, A.; Iravani, P. Understanding LSTM network behaviour of IMU-based locomotion mode recognition for applications in prostheses and wearables. *Sensors* **2021**, *21*, 1264. [CrossRef]
8. Brantley, J.A.; Luu, T.P.; Nakagome, S.; Contreras-Vidal, J.L. Prediction of lower-limb joint kinematics from surface EMG during overground locomotion. In Proceedings of the 2017 IEEE International Conference on Systems, Man, and Cybernetics (SMC), Banff, AB, Canada, 5–8 October 2017.
9. Bhakta, K.; Camargo, J.; Young, A.J. Control and experimental validation of a powered knee and ankle prosthetic device. In Proceedings of the ASME 2018 Dynamic Systems and Control Conference, Atlanta, GA, USA, 30 September–3 October 2018.
10. Simon, A.M.; Finucane, S.B.; Ikeda, A.J.; Cotton, R.J.; Hargrove, L.J. Powered knee and ankle prosthesis use with a K2 level ambulator: A case report. *Front. Rehabil. Sci.* **2023**, *4*, 1203545. [CrossRef]
11. Pi, M. Gait control of robotic leg prosthesis based on motion predictive system. In Proceedings of the International Conference on Advanced Robotics and Mechatronics, Shenzhen, China, 18–21 December 2020.
12. Zhang, K.; Xiong, C.; Zhang, W.; Liu, H.; Lai, D.; Rong, Y.; Fu, C. Environmental features recognition for lower limb prostheses toward predictive walking. *IEEE Trans. Neural Syst. Rehabil. Eng.* **2019**, *27*, 465–476. [CrossRef]
13. Stolyarov, R.; Carney, M.; Herr, H. Accurate heuristic terrain prediction in powered lower-limb prostheses using onboard sensors. *IEEE Trans. Biomed. Eng.* **2021**, *68*, 384–392. [CrossRef]
14. Mazón, D.M.; Groefsema, M.; Lambert, R.B.; Carloni, R. IMU-based classification of locomotion modes, transitions, and gait phases with convolutional recurrent neural networks. *Sensors* **2022**, *22*, 8871. [CrossRef]
15. Barberi, F.; Iberite, F.; Anselmino, E.; Randi, P.; Sacchetti, R.; Gruppioni, E.; Mazzoni, A.; Micera, S. Early decoding of walking tasks with minimal set of EMG channels. *J. Neural Eng.* **2023**, *20*, 026038. [CrossRef]
16. Zhou, C.; Yang, L.; Liao, H.; Liang, B.; Ye, X. Ankle foot motion recognition based on wireless wearable sEMG and acceleration sensors for smart AFO. *Sens. Actuator A Phys.* **2021**, *331*, 113025. [CrossRef]
17. Meng, L.; Pang, J.; Wang, Z.; Xu, R.; Ming, D. The role of surface electromyography in data fusion with inertial sensors to enhance locomotion recognition and prediction. *Sensors* **2021**, *331*, 6291. [CrossRef]
18. Hu, B.; Rouse, E.; Hargrove, L. Benchmark Datasets for bilateral lower-limb neuromechanical signals from wearable sensors during unassisted locomotion in able-bodied individuals. *Front. Robot. AI* **2018**, *5*, 14. [CrossRef]
19. Fleming, A.; Huang, S.; Huang, H. Proportional myoelectric control of a virtual inverted pendulum using residual antagonistic muscles: Toward voluntary postural control. *IEEE Trans. Neural Syst. Rehabil. Eng.* **2019**, *27*, 1473–1482. [CrossRef]
20. Huang, S.; Huang, H. Voluntary control of residual antagonistic muscles in transtibial amputees: Reciprocal activation, coactivation, and implications for direct neural control of powered lower limb prostheses. *IEEE Trans. Neural Syst. Rehabil. Eng.* **2019**, *27*, 85–95. [CrossRef]
21. Turner, S.; McGregor, A.H. Perceived effect of socket fit on major lower limb prosthetic rehabilitation: A clinician and amputee perspective. *Arch. Rehabil. Res. Clin. Transl.* **2020**, *2*, 100059. [CrossRef]
22. Safari, M.R.; Meier, M.R. Systematic review of effects of current transtibial prosthetic socket designs—Part 1: Qualitative outcomes. *J. Rehabil. Res. Dev.* **2015**, *52*, 491–508. [CrossRef]
23. Trigno Avanti Sensor. Available online: <https://delsys.com/trigno-avanti/> (accessed on 11 October 2023).
24. Ministerio de Vivienda, Construcción y Saneamiento del Gobierno Peruano. Accesibilidad Para Personas con Discapacidad y de las Personas Adultas Mayores. Available online: [https://www.mimp.gob.pe/adultomayor/archivos/Norma\\_A\\_120.pdf](https://www.mimp.gob.pe/adultomayor/archivos/Norma_A_120.pdf) (accessed on 11 October 2023).
25. Nazmi, N.; Abdul Rahman, M.A.; Yamamoto, S.-I.; Ahmad, S.A. Walking gait event detection based on electromyography signals using artificial neural network. *Biomed. Signal Process. Control* **2018**, *47*, 334–343. [CrossRef]
26. Toledo-Pérez, D.C.; Rodríguez, J.; Gómez, R.A.; Martínez, J.F.; Carrasco, J.A. Feature selection algorithms to reduce processing time in classification with SVMs. In Proceedings of the XVII International Engineering Congress, Queretaro, Mexico, 14–18 June 2021.
27. Trigini, A.; Scattolini, M.; Mengarelli, A.; Fioretti, S.; Morettini, M.; Burattini, L.; Verdini, F. Role of the Window Length for Myoelectric Pattern Recognition in Detecting User Intent of Motion. In Proceedings of the 2022 IEEE International Symposium on Medical Measurements and Applications (MeMeA), Messina, Italy, 22–24 June 2022.
28. Trigini, A.; Al-Timemy, A.; Verdini, F.; Fioretti, S.; Morettini, M.; Burattini, L.; Mengarelli, A. Decoding transient sEMG data for intent motion recognition in transhumeral amputees. *Biomed. Signal Process. Control* **2023**, *85*, 104936. [CrossRef]
29. Kopke, J.V.; Ellis, M.D.; Hargrove, L.J. Determining User Intent of Partly Dynamic Shoulder Tasks in Individuals with Chronic Stroke Using Pattern Recognition. *IEEE Trans. Neural Syst. Rehabil. Eng.* **2019**, *28*, 350–358. [CrossRef]
30. Sarshar, M.; Polturi, S.; Schega, L. Gait Phase Estimation by Using LSTM in IMU-Based Gait Analysis—Proof of Concept. *Sensors* **2021**, *21*, 5749. [CrossRef]
31. Camargo, J.; Flanagan, W.; Csomay-Shanklin, N.; Kanwar, B.; Young, A. A Machine Learning Strategy for Locomotion Classification and Parameter Estimation Using Fusion of Wearable Sensors. *IEEE Trans. Biomed. Eng.* **2021**, *68*, 350–358. [CrossRef]
32. Huang, H.; Zhou, P.; Li, G.; Kuiken, T.A. An Analysis of EMG Electrode Configuration for Targeted Muscle Reinnervation Based Neural Machine Interface. *IEEE Trans. Neural Syst. Rehabil. Eng.* **2008**, *16*, 37–45. [CrossRef]

33. Bruinsma, J.; Carloni, R. IMU-based deep neural network: Prediction of locomotor and transition intentions of an osseointegrated transfemoral amputee. *IEEE Trans. Neural Syst. Rehabil. Eng.* **2021**, *29*, 1079–1088. [[CrossRef](#)]
34. Putri, F.T.; Caesarendra, W.; Królczyk, G.; Glowacz, A.; Prawibowo, H.; Ismail, R.; Indrawati, R.T. Human walking gait classification utilizing an artificial neural network for the ergonomics study of lower limb prosthetics. *Prosthesis* **2023**, *5*, 647–665. [[CrossRef](#)]

**Disclaimer/Publisher’s Note:** The statements, opinions and data contained in all publications are solely those of the individual author(s) and contributor(s) and not of MDPI and/or the editor(s). MDPI and/or the editor(s) disclaim responsibility for any injury to people or property resulting from any ideas, methods, instructions or products referred to in the content.